ResearchGate

See discussions, stats, and author profiles for this publication at: https://www.researchgate.net/publication/263015786

Simple, Sensitive, and Quantitative Electrochemical Detection Method for Paper Analytical Devices

ARTICLE *in* ANALYTICAL CHEMISTRY · JUNE 2014

Impact Factor: 5.64 · DOI: 10.1021/ac501004a · Source: PubMed

CITATIONS
9

READS
67

5 AUTHORS, INCLUDING:

Karen Scida
3M
14 PUBLICATIONS **220** CITATIONS

SEE PROFILE

Josephine Cunningham
University of Texas at Austin
7 PUBLICATIONS **145** CITATIONS

SEE PROFILE

Available from: Karen Scida
Retrieved on: 01 February 2016

analytical chemistry

Article

pubs.acs.org/ac

Simple, Sensitive, and Quantitative Electrochemical Detection Method for Paper Analytical Devices

Karen Scida,[†] Josephine C. Cunningham,[†] Christophe Renault,[†] Ian Richards,[‡] and Richard M. Crooks*,[†]

[†]Department of Chemistry and Biochemistry and the Center for Nano- and Molecular Science and Technology, The University of Texas at Austin, 105 East 24th Street, Stop A5300, Austin, Texas 78712-1224, United States

[‡]Interactives Executive Excellence LLC, 201 North Weston Lane, Austin, Texas 78733, United States

Supporting Information

ABSTRACT: We report a new type of paper analytical device that provides quantitative electrochemical output and detects concentrations as low as 767 fM. The model analyte is labeled with silver nanoparticles (AgNPs), which provide 250 000-fold amplification. AgNPs eliminate the need for enzymatic amplification, thereby improving device stability and response time. The use of magnetic beads to preconcentrate the AgNPs at the detection electrode further improves sensitivity. Response time is improved by incorporation of a hollow channel, which increases the flow rate in the device by a factor of 7 and facilitates the use of magnetic beads. A key reaction necessary for label detection is made possible by the presence of a slip layer, a fluidic switch that can be actuated by manually slipping a piece of paper. The design of the device is versatile and should be useful for detection of proteins, nucleic acids, and microbes.

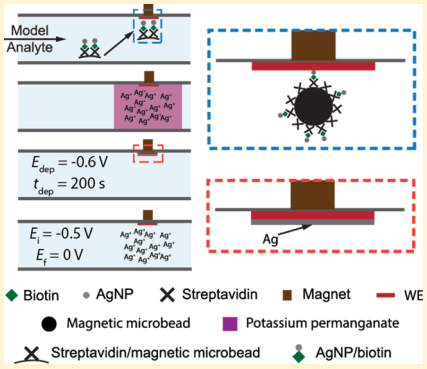

Here we report a novel paper-based analytical device (PAD) that provides for timed reactions, quantitative electrochemical detection,[1−3] simple assembly by folding the paper substrate,[4] and fast, robust, nonenzymatic signal amplification. These all represent significant advances for the field of low-cost diagnostics, because, as we will show, they provide important functionality without significantly increasing device complexity. For example, one particularly important feature of the device is that it employs a hollow channel.[5,6] In contrast to channels filled with cellulose fibers, hollow channels do not impede micrometer-scale magnetic beads, and the latter provide a simple means for localizing a labeled target in the vicinity of a detection electrode. In this case, the labels are ∼20 nm diameter Ag nanoparticles (AgNPs). The device also incorporates a fluidic switch,[7,8] which makes it possible to localize and time a key, on-device, homogeneous reaction that is required for signal amplification. Integration of these new functionalities results in a low-cost, quantitative, paper-only diagnostic tool that yields a detection limit of <1 pM of AgNP labels.

Ultralow-cost, paper-based diagnostic tools offer an effective solution to healthcare accessibility problems in developing nations as well as providing convenient medical information to individuals in more affluent societies. However, there are a number of scientific and engineering barriers to the large-scale adoption of next-generation PADs that have stimulated much recent research in this field.[9−11] Of course, the particular challenges required for a PAD depends on the specific application, but the expanded use of such tools would be accelerated by some or all of the following: lowered limits of detection (LOD), increased sensitivity and dynamic range, detection strategies that provide quantitative information, reduced nonspecific adsorption (NSA), reduced analysis time, robust recognition probes, superior manufacturability, lower cost, and simplified user interfaces. The advances reported here address several of these challenges, but the main focus is on quantitation and lowered LODs employing a user-friendly platform.

PAD-based assays that require low LODs must incorporate some form of chemical amplification.[12] To maintain the advantage of the PAD format, such amplification should be simple and robust. One such amplification method relies on paper supercapacitors to store charge, which can subsequently be released instantaneously to achieve gain.[13] Likewise, nanoporous gold has been used as an amplification platform for the capture of target DNA functionalized with an electroactive molecule.[14] Gold nanoparticle labels have been used as catalysts for a subsequent electroless deposition amplification step,[15] enzyme-linked immunosorbent assay (ELISA) reagents were dried and stored on a two-dimensional paper network that automated the ELISA steps for the detection of malarial biomarkers,[16] and CuO NP labels have been used to trigger fluorescence from quantum dots.[17] Phillips and co-workers designed a timed-colorimetry assay based on the differences in flow rates in the presence and absence of an enzyme and achieved detection limits for enzymes in the femtomolar range.[18] In addition to these examples, other amplification approaches have been reported but in our opinion

Received: March 19, 2014
Accepted: May 21, 2014
Published: June 11, 2014

 © 2014 American Chemical Society

they are generally specialized for particular targets or too complicated for simple PAD-based point-of-care (POC) applications.[19,20]

In this article, we present an easily fabricated paper-based platform having a simple user interface and a demonstration of its operation using a model target analyte. The detection method involves two simple, but effective, preconcentration steps. The first of these involves magnetic preconcentration of AgNP labels at a working electrode, followed by the spontaneous oxidation of these labels in the presence of $KMnO_4$.[21,22] Importantly, this oxidizing agent is delivered into the channel at a specific time and location by simply slipping a moveable piece of paper that is part of the device. The resulting Ag^+ can then be electrodeposited as zerovalent Ag onto the working electrode. This represents a second kind of preconcentration, and hence oxidation of this Ag layer, using anodic stripping voltammetry (ASV), leads to very sensitive detection of the AgNP-labeled target.[23] The entire assay takes just 4.6 min, is quantitative, and allows detection of label concentrations as low as 767 fM.

■ EXPERIMENTAL SECTION

Chemicals and Materials. Sodium phosphate monobasic, sodium phosphate dibasic, biotin (5-fluorescein) conjugate, microtiter plates (Corning 3650), and $KMnO_4$ were purchased from Sigma-Aldrich (St. Louis, MO). NaCl, NaOH, Whatman grade 1 chromatography paper (180 μm thick, 20 cm × 20 cm, linear flow rate (water) of 13 cm/30 min), microcentrifuge tubes, and two-part 5 min epoxy were purchased from Fisher Scientific (Pittsburgh, PA). AlexaFluor-647/streptavidin conjugate was purchased from Life Technologies (Grand Island, NY). Streptavidin-coated magnetic microbeads (2.8 μm in diameter) were obtained from Bangs Laboratories (Fishers, IN). Biotinylated DNA (5′d Thiol C6 SS-ACATTAAAATTC-Biotin 3′) was acquired as a powder from Biosearch Technologies (Petaluma, CA) and, before use, was dissolved in the appropriate volume of deionized water to yield a concentration of 100.0 μM. A 1.0 M stock phosphate buffer solution was prepared by dissolving the appropriate amount of sodium phosphate monobasic and sodium phosphate dibasic in 0.5 L of deionized water and adjusting to the desired pH with NaOH. Erioglaucine disodium salt (blue dye) was obtained from Acros Organics (Pittsburgh, PA). Conductive carbon paste (Cl-2042) was purchased from Engineered Conductive Materials (Delaware, OH). All solutions were prepared with deionized water (<18.0 MΩ cm, Milli-Q Gradient System, Millipore, Bedford, MA).

Citrate-capped AgNPs, nominally 20 nm in diameter (measured size, 21 ± 1 nm, Figure S3 in the Supporting Information), were from Ted Pella (Redding, CA). They were modified with biotinylated DNA following a protocol by Alivisatos and co-workers.[24] Details are provided in the Supporting Information. The preparation of the AgNP/biotin/streptavidin/magnetic microbead model analyte, and conjugation of streptavidin-coated magnetic microbeads with biotin-modified fluorescein, are described in the Supporting Information. A 1/16 in. × 1/2 in. neodymium cylindrical magnet (N48) was purchased from Apex Magnets (Petersburg, WV). Acrylic plates (0.6 cm-thick) were obtained from Evonik Industries (AcryliteFF). Clear nail polish was purchased from Electron Microscopy Sciences (Hatfield, PA). Copper epoxy (EPO-TEK 430) was acquired from Epoxy Technology (Billerica, MA). Conductive copper tape (6.3 mm wide) was from Ted Pella.

Instrumentation. All electrochemical measurements were performed using a bipotentiostat (700E, CH Instruments, Austin, TX). A polytetrafluoroethylene electrochemical cell was used for conventional electrochemical measurements. These experiments were performed using a glassy carbon working electrode (1.0 mm diameter), Ag/AgCl reference electrode (KCl = 1 M), and Pt wire counter electrode (CH Instruments, Austin, TX). The cell is shown in Figure S1 in the Supporting Information. The size of the citrate-capped AgNPs was characterized via Nanoparticle Tracking Analysis (NS500, Nanosight). The modification of AgNPs with biotinylated DNA was carried out using microtiter plates and these were analyzed for fluorescence using EnVision (PerkinElmer). UV–vis measurements were made with a Hewlett-Packard HP8453 spectrometer using a quartz cell (l = 10 mm, 50 μL) from Starna Cells (Atascadero, CA). A Sorvall Legend Micro 21R Centrifuge (Thermo Scientific) was used in the synthesis of biotinylated AgNPs. Mixing of all solutions was performed with a Mini Vortexer 945300 (VWR Scientific Products). The stencil was cut using an Epilog laser engraving system (Zing 16). Vacuum centrifugation was achieved with a Thermo Savant DNA120 SpeedVac Concentrator. Wax printing was carried out with a Xerox ColorQube 8570DN inkjet printer.

***o*Slip Fabrication.** The *o*Slip patterns (Figure S2 in the Supporting Information) were designed using Adobe Illustrator CS6 (version 16.0.0) and printed on Whatman grade 1 chromatography paper using the wax printer.[25,26] Next, the paper sheet was placed in an oven at 130 °C for 50 s to melt the wax and form three-dimensional hydrophobic walls. Note that the hydrophilic part of Layer 4 (yellow section of Figure S2 in the Supporting Information) was constructed by applying 60% yellow wax.[5] After the paper was removed from the oven and cooled to 25 °C, each individual device was cut from the paper sheet using scissors and the white sections surrounded by the orange lines in Figure S2 in the Supporting Information were removed using a razor blade.

The stencil for printing the electrodes was designed (Figure S2 in the Supporting Information) using Adobe Illustrator CS6 (version 16.0.0) and cut into transparency films using the laser engraving system. The finalized stencil was aligned with Layer 1 as shown in Figure S2 in the Supporting Information and thickened carbon paste (see the Supporting Information) was spread on top of the stencil using a scraper. The stencil printed carbon paste was then left to dry at 25 °C for 1 h. A total of 20 devices could be stencil printed at the same time with the current setup. Using a procedure described in the Supporting Information, electrical contacts were added to the electrodes. Finally, the blue dye and $KMnO_4$ were dispensed onto locations of the *o*Slip, as described later.

■ RESULTS AND DISCUSSION

Electrochemical Characterization of AgNP Detection Using a Conventional Electrochemical Cell. The electrochemical detection method, which is a key feature of the *o*Slip, involves three steps: oxidation of AgNPs using MnO_4^-, reduction of the resulting Ag^+ onto an electrode surface, and ASV to quantitate the number of AgNP labels originally present. To ensure the viability of this method, and to ensure optimized performance, we tested the basic principles using a conventional electrochemical cell prior to translating the approach to the *o*Slip. The electrochemical cell used for these

experiments is shown in Figure S1a in the Supporting Information. It is conventional, except that the glassy carbon working electrode is inserted into the bottom of the cell such that the electrode surface faces up. This arrangement, which we refer to as the *Facing up* configuration, was used because of the very small sample volumes.

The experiment was carried out as follows. First, the electrolyte, consisting of 125.0 μL of 100.0 mM phosphate buffer (pH 7.4) containing 100.0 mM NaCl (this buffer is referred to hereafter as PBCl) and 50.0 μL of 187.0 μM $KMnO_4$, were added to the test cell. Second, 50.0 μL of an aqueous solution containing citrate-capped AgNPs were added. Under these conditions, MnO_4^- (E° = 1.18 V vs NHE at pH 7.4)[27] should oxidize the AgNPs to Ag^+ (E° = 0.16 V vs NHE in the presence of 100 mM Cl^-).[28] Importantly, there are ~250 000 Ag atoms in one AgNP, which results in 250 000 equiv of charge for every AgNP. Third, after 30 s, the working electrode was held at −0.300 V for 200 s to electrodeposit Ag. Finally, the potential was held at 0 V for 10 s and then swept from E_i = 0 to E_f = 0.200 V at υ = 10 mV/s to electrochemically oxidize Ag to Ag^+.

The ASVs resulting from the foregoing experiment are shown in Figure 1a. There are three important observations. First, Figure S3 in the Supporting Information confirms oxidation of the AgNPs by MnO_4^-, and Figure 1a shows that electrodeposition of Ag followed by anodic stripping results in an easily detectable signal even at concentrations as low as 3.3 pM. Second, the calibration curve in Figure 1b reveals a linear correlation between the charge measured under the ASV peaks and the concentration of AgNPs over the range from 3.3 to 25 pM. The nonlinear part of the curve probably arises from the use of a fixed (and for the two data points at high AgNP concentration, substoichiometric) concentration of the MnO_4^- oxidant. Third, the presence of a high (100 mM) concentration of Cl^- and PO_4^{3-} in the buffer solution does not result in observable precipitation of AgCl or Ag_3PO_4 (Figure S4 in the Supporting Information) . We believe this is because the presence of MnO_4^- enhances the solubility of Ag^+.

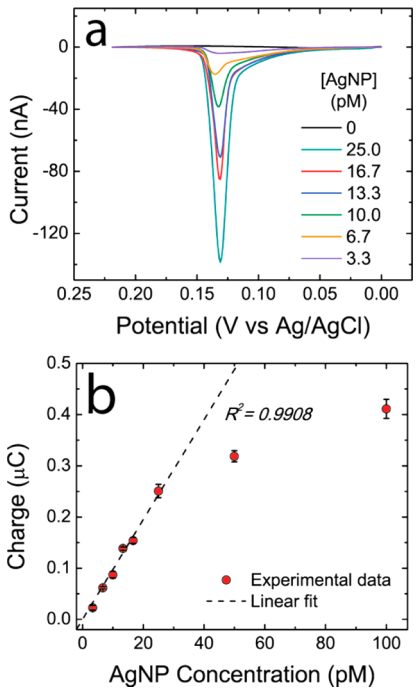

Figure 1. Electrochemical results, obtained using a conventional electrochemical cell (Figure S1 in the Supporting Information), demonstrating the viability of the detection strategy used in the *o*Slip platform. (a) ASV corresponding to samples containing 0 to 25 pM citrate-capped AgNPs (nominally 20 nm). The data were corrected for a sloping baseline. The working electrode was glassy carbon (1.0 mm diameter) and the electrolyte consisted of 125.0 μL of PBCl. υ = 10 mV/s. (b) Calibration curve showing the relationship between the charge, measured under the ASV peaks, and the AgNP concentration introduced to the cell. The black dashed-line is the best linear fit of the experimental data. The error bars for each data point represent the standard deviation for three different measurements.

Description and Assembly of the *o*Slip. The device shown in Scheme 1, which we call an *o*Slip, is intended to provide a versatile design strategy for detecting a range of targets, including nucleic acids, proteins, and microbes. The *o*Slip is composed of 4 layers (Scheme 1a). Layer 1 contains two paper reservoirs called the Inlet and the Outlet. Layer 2 has a large rectangular paper section and a smaller circular paper reservoir. Layer 3 (the Slip layer) consists of a large rectangular paper section and two smaller paper reservoirs, one circular and the other square. Finally, Layer 4 contains a hydrophilic layer (yellow rectangle) and an oval Sink pad.

After the patterns are wax-printed, the Inlet of Layer 1 and the large rectangular sections of Layers 2 and 3 are removed using a razor blade (Figure S2 in the Supporting Information). Next, 2.0 mm-diameter carbon electrodes are stencil printed on Layer 1 using a protocol described in the Experimental Section and in the Supporting Information. The electrodes in Scheme 1a are just to the left of the labels WE, RE, and CE, which refer to the working, reference, and counter electrodes, respectively. Next, 3.0 μL of a concentrated aqueous solution of a blue dye is drop cast and dried onto the circular paper reservoir of Layer 2, and 4.0 μL of a 934 μM aqueous solution of $KMnO_4$ is drop cast and dried onto the square reservoir on Layer 3 (Scheme 1a). At this point, the *o*Slip is assembled (Scheme 1b) by folding Layers 1, 2, and 4, so that the face of Layer 1 supporting the carbon electrodes, as well as the hydrophilic section of Layer 4, are in contact with opposite faces of Layer 2. Subsequently, Layer 3 (the Slip layer) is placed between Layers 2 and 4 such that the circular reservoir of Layer 2 and the Sink pad of Layer 4 are aligned with the circular reservoir of Layer 3.

After assembly, the void spaces present in Layers 1, 2, and 3, together with the hydrophilic section of Layer 4, constitute a single hollow channel. The hydrophilic floor of this channel in Layer 4 is very important, because it ensures flow (a mixture of capillary and low-pressure flow) through the hollow channel.[5] The resulting alignment of all layers is represented in Scheme 1c, which is a cross-sectional cut of the *o*Slip across the length of the channel (red-dashed line in Scheme 1b). Note that the layers are numbered from top to bottom in Scheme 1a, following the order of liquid flow through the device as shown in Scheme 1c (top). Finally, the *o*Slip is placed inside a holder, consisting of two acrylic plates that compress the device using paper binder clips, and a small magnet is placed in a close-fitting hole present in the top acrylic plate. This ensures that the magnet is aligned with the WE, as shown in Scheme 1c,d.

Operation of the *o*Slip. We tested the operation of the *o*Slip using a conjugate consisting of biotin/streptavidin labeled with nominally ~20 nm AgNPs and 2.8 μm magnetic microbeads. Hereafter, this conjugate is referred to as the "model analyte", and its preparation is described in the Supporting Information. The operation of the *o*Slip was tested

Scheme 1

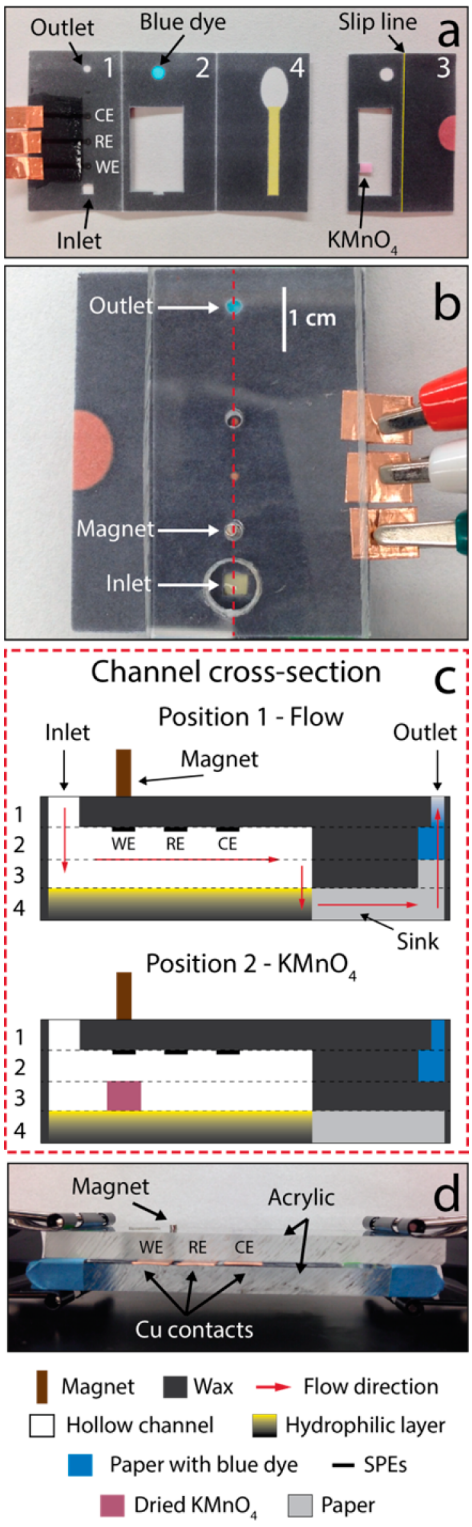

by adding 50.0 μL of PBCl buffer containing different concentrations of the model analyte to the Inlet while the Slip layer is in position 1 (Scheme 1c). In this configuration, the sample flows horizontally across the hollow channel and the model analyte is concentrated at the working electrode by the magnetic field (first preconcentration step, Scheme 2a, also see blue-border inset). The PBCl buffer and any other components of the sample not conjugated to magnetic microbeads flow further through the channel and into the Sink.

Scheme 2

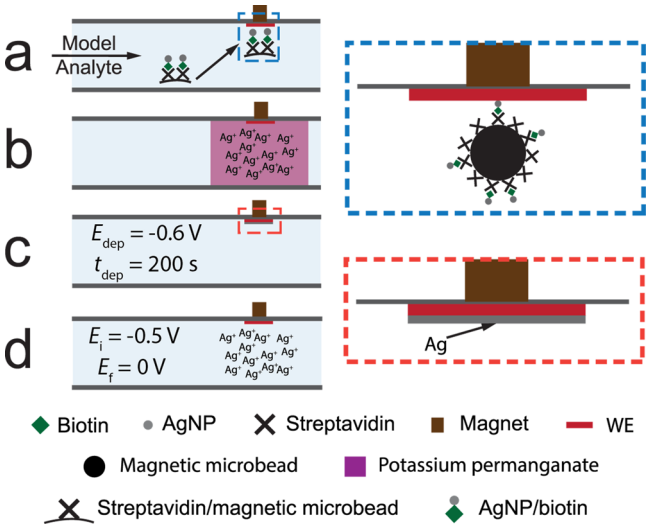

When the Sink becomes saturated with buffer, upward flow is initiated through the device (Scheme 1c, top). This upward flow picks up the preloaded blue dye on Layer 2 and causes the Outlet to turn blue in 15 ± 2 s (Movie S1 in the Supporting Information). This indicates that flow inside the hollow channel has ceased. At this point, Layer 3 is pulled into position 2 by aligning the yellow Slip line (Scheme 1a) with the edge of the holder (see Movie S1 in the Supporting Information). This results in placement of the square reservoir on Layer 3, which contains predispensed and dried $KMnO_4$, directly beneath the WE (Scheme 1c, bottom). The dissolved MnO_4^- then diffuses to the AgNPs trapped under the WE and oxidizes them to Ag^+. The second preconcentration step is initiated 12 s after moving the Slip layer into position 2: the WE is held at $E = -0.600$ V vs the carbon-paste quasi-reference electrode (cpQRE) for $t = 200$ s to electrodeposit Ag onto the WE ($Ag^+ + e = Ag$, Scheme 2c, also see red-border inset). Finally, the electrode potential is held at −0.500 V for 10 s, and then it is swept from $E_i = -0.500$ V to $E_f = 0$ V at $\upsilon = 10$ mV/s. This results in the anodic current transient corresponding to oxidation of Ag into Ag^+ (Scheme 2d).

It is important to mention that conditions of no flow need to be met before slipping Layer 3 into position 2 (i.e., when the *Outlet* turns blue) in order to, first, constrain the resolvated MnO_4^- close to the *WE* so that it oxidizes the previously concentrated AgNP labels to Ag^+ ions (Scheme 2b), and second, confine the resulting Ag^+ in close proximity to the WE (Scheme 2d) so that charge collection during the electrodeposition step is efficient.

Characteristics of the *o*Slip. The maximum charge obtained in the *o*Slip was optimized by varying the number of moles of MnO_4^-, while keeping the number of AgNPs constant. This experiment was carried out by dispensing and drying different number of moles of MnO_4^- onto the location of the *o*Slip noted in Scheme 1. Next, 3.0 μL of the model analyte stock solution (containing 908 pM AgNP) was added to the Inlet, followed immediately by 47.0 μL of PBCl buffer. The rest of the procedure was the same as that described in the previous section.

dx.doi.org/10.1021/ac501004a | *Anal. Chem.* 2014, 86, 6501−6507

Figure 2 shows that the amount of Ag collected at the electrode increases with the amount of MnO_4^- dried in the device until it reaches a maximum, and then it decreases. This maximum is observed at 3.7 nmol of MnO_4^-. Therefore, all the *o*Slip experiments were carried out using this amount of the oxidizing agent. It is, however, worth noting that to the left of the maximum in Figure 2, there are insufficient MnO_4^- equivalents available to fully oxidize the AgNPs. To the right of the maximum point, the use of increasing MnO_4^- concentrations results in the formation of thicker layers of MnO_2 on the WE.[33,34] This insoluble solid electrically insulates the electrode surface and inhibits Ag reduction and subsequent reoxidation (see Figure S8 in the Supporting Information).

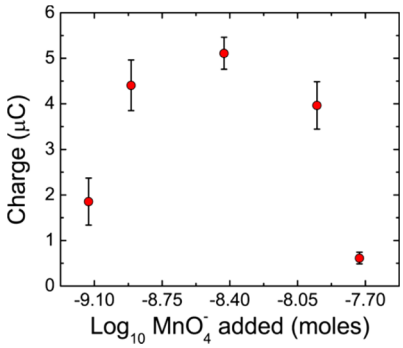

Figure 2. Optimization of the electrochemical signal in the *o*Slip. Plot of charge under the ASV peak as a function of the number of moles of MnO_4^- added. The number of moles of Ag was kept constant. The error bars represent the standard deviation for three different measurements.

The capture efficiency of the model analyte at the WE is an important parameter that directly affects the LOD of the assay. We measured this efficiency by adding 50.0 μL of PBCl-containing 0.20 pM fluorescein-labeled magnetic microbeads (used as a proxy for the model analyte) to the Inlet of an assembled *o*Slip (full details of this experiment are provided in the Supporting Information). After the solution evaporated, the *o*Slip was unfolded and the fluorescence at the WE was measured. A control experiment was carried out by dispensing the same number of moles of the labeled microbeads directly onto the WE of an unassembled device, and the fluorescence was measured. As shown in Figure 3a, 84 ± 14% of the fluorescence measured in the control experiment is obtained in the flow/capture test. Figure 3b,c shows fluorescence micrographs of the type used as the basis for the test and control histograms, respectively, represented in Figure 3a. The orange dashed-lines highlight the outline of the carbon stencil-printed electrodes, while the yellow lines show the region-of-interest from which the fluorescence intensities were obtained. This region-of-interest was placed at a section of the WE where the fluorescence intensity was highest. These experiments are important because they demonstrate that the vast majority of the model analyte is preconcentrated at the WE before MnO_4^- is introduced to the system, thereby validating the first preconcentration principle that is key to the operation of the *o*Slip.

Performance of the *o*Slip. Figure 4a shows ASV peaks resulting from analysis of different concentrations of the model analyte by the *o*Slip. The area under these peaks corresponds to the total charge resulting from AgNP oxidation, and hence it should be correlated to the concentration of the model analyte

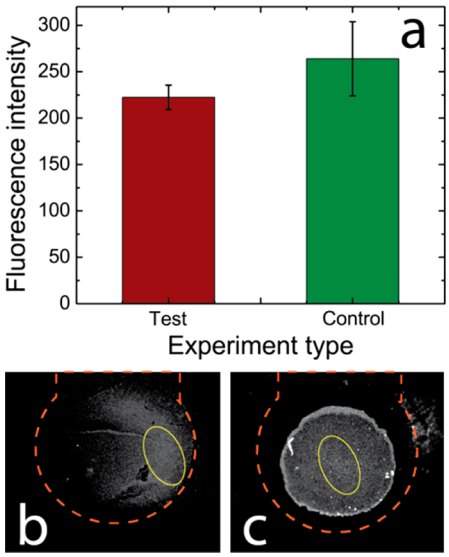

Figure 3. Fluorescence experiments performed to calculate the capture efficiency of 2.8 μm-diameter fluorescein-modified magnetic microbeads on the working electrode (WE) of the *o*Slip. (a) Histogram comparing the fluorescence obtained in control and test experiments. Each type of experiment was background corrected (Figure S5 in the Supporting Information) and performed in triplicate. Fluorescence micrographs of the WE for (b) one of the test experiments and (c) one of the control experiments. The orange-dashed and solid yellow lines in parts b and c represent the location of the WE and the areas used to measure the fluorescence intensity, respectively. Note that equivalent areas were used to measure the fluorescence intensity in parts b and c.

introduced to the *o*Slip. Indeed, Figure 4b shows that this correlation is linear, demonstrating that both the device platform and electrochemical detection method function as anticipated by Schemes 1 and 2.

The electrochemical response shown in Figure 4b indicates good analytical sensitivity (slope = $1.03 \times 10^{-7} \pm 2 \times 10^{-9}$ C/pM). The lowest detectable concentration of AgNP labels, shown by the pink line in the inset of Figure 4a, is 767 fM. In addition, the charge collection efficiency (defined as the average absolute charge detected divided by the charge originally added) is 13 ± 2%, and the linear range is from 0.77 to 36.8 pM.

When performing the *o*Slip experiment in the absence of MnO_4^-, no anodic stripping signal is observed even at AgNP concentrations as high as 55.3 pM. This is because lack of electrical contact between the AgNP labels and the electrode surface in the absence of MnO_4^- (Scheme 2, blue-border inset) results in poor detection sensitivity. Indeed, this is the reason for using MnO_4^- to enable AgNP signal amplification.

The device-to-device reproducibility for the *o*Slip is remarkably good considering how simple it is and the limited number of replicates that have been carried out so far. Specifically, the relative standard deviation of the signal (RSD, defined as the standard deviation divided by the mean signal intensity) is 13 ± 4% determined for 16 independently prepared *o*Slips. This value was obtained from the average RSD of different data points in the calibration curve linear range.

One final point: the signal output of the *o*Slip is obtained in only 4.6 min, which includes a Ag electrodeposition time of 200 s. Longer electrodeposition times (e.g., t = 500 s) could result in detection of lower concentrations but would add to the total

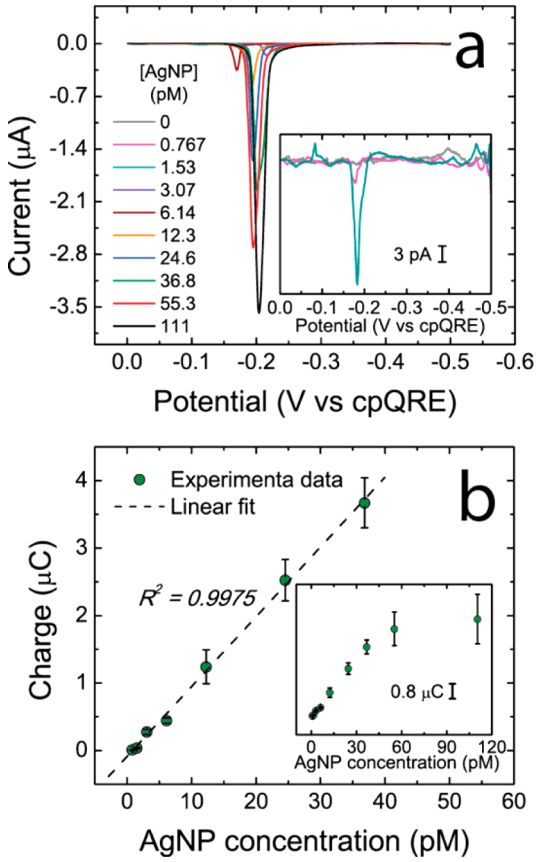

Figure 4. Electrochemical results obtained using the model analyte in the *o*Slip. (a) ASV peaks as a function of the concentration of AgNPs introduced at the Inlet of the device. The inset shows the ASV peaks corresponding to the background and AgNP concentrations of 767 fM and 1.53 pM. The data were corrected for a sloping baseline. The electrolyte, working electrode (WE), and sweep rate were 50.0 μL PBCl, carbon stencil-printed (2.0 mm diameter), and 10 mV/s, respectively. The ohmic drop (4170 ± 360 Ω, for 15 devices) was corrected for each *o*Slip. (b) Calibration curve relating total measured charge to the concentration of AgNP labels introduced at the Inlet. The black dashed-line is the best linear fit of the experimental data. The inset shows the linear range and two additional data points (55.3 and 111 pM) demonstrating deviation from linearity at high AgNP concentration. The error bars for each data point represent the standard deviation of the signal obtained for three different *o*Slips.

analysis time. Hence, depending on the intended assay, the time-to-answer can be offset against the target LOD.

■ SUMMARY AND CONCLUSION

In conclusion, we have reported a new family of paper-based sensors that are very well suited for POC applications. This device, the *o*Slip, is inexpensive (~$1 per device at the unoptimized lab fabrication scale), amenable to simple and rapid fabrication techniques, user-friendly (electrochemical detection and no washing steps), sensitive, portable, quantitative, robust (AgNPs, rather than enzymes, as the source of amplification), efficient (composite capture efficiency of 84 ± 14% and charge collection efficiency of 13 ± 2%), sufficiently fast for many applications (completion of analysis in 4.6 min), and can detect low label concentrations (767 fM). These desirable attributes are a consequence of thoughtful integration of recent innovations, including hollow channels, the SlipPAD, and a novel electrochemical amplification strategy. In keeping with the philosophy of simplicity, which is inherent to the paper POC design paradigm, the only actions required by the user to carry out an assay are placement of the sample onto the device and then moving the Slip layer when signaled by the device to do so.

The conditions under which the proof-of-concept experiment were carried out (neutral pH and a NaCl concentration of 100 mM) are similar to those present in human urine,[29] which is a potential sample matrix for a wide variety of bioassays. Because of the filtering ability of paper, it is also likely that the assay could be configured for use with whole blood samples.[30] We believe the proposed platform will be highly flexible, in that bioassays for nucleic acids, proteins, and even microbes can be designed without significantly changing the basic device design.[31,32] Specific assays are currently being developed, and the outcomes will be reported in due course.

■ ASSOCIATED CONTENT

Supporting Information

Experimental section including instrumentation and protocols for biotinylation of AgNPs, preparation of the model analyte, modification of magnetic microbeads with fluorescein, ASVs obtained using the conventional electrochemical setup, thickening of carbon ink for stencil printing, adding electrical contacts to the stencil-printed electrodes, reagent loading on the *o*Slip, and drying conditions for measuring the capture efficiency of the model analyte at the WE; results for two different conventional electrochemical configurations; a scheme showing the detailed architecture of the *o*Slip; additional evidence for the spontaneous oxidation of AgNPs by MnO_4^-; effect of Cl^- and PO_4^{3-} on the electrochemical signal; micrographs showing the background fluorescence of the *o*Slip WE; UV−vis spectra demonstrating formation of the model analyte; optimization of the electrochemical signal using the conventional electrochemical setup; evidence for the electrical insulation of the electrode with MnO_2; optimization of MnO_4^- resolvation in the *o*Slip. This material is available free of charge via the Internet at http://pubs.acs.org.

■ AUTHOR INFORMATION

Corresponding Author

*E-mail: crooks@cm.utexas.edu. Phone: 512-475-8674.

Notes

The authors declare no competing financial interest.

■ ACKNOWLEDGMENTS

This project is sponsored by the Department of the Defense, Defense Threat Reduction Agency (Contract Number HDTRA-1-13-1-0031). R.M.C. thanks the Robert A. Welch Foundation (Grant F-0032) for sustained research support. J.C.C. thanks the NASA Harriett G. Jenkins Graduate Fellowship Program, a NASA Office of Education Minority University Research and Education Program (MUREP).

■ REFERENCES

(1) Dungchai, W.; Chailapakul, O.; Henry, C. S. *Anal. Chem.* **2009**, *81*, 5821−5826.

(2) Santhiago, M.; Wydallis, J. B.; Kubota, L. T.; Henry, C. S. *Anal. Chem.* **2013**, *85*, 5233−5239.

(3) Noiphung, J.; Songjaroen, T.; Dungchai, W.; Henry, C. S.; Chailapakul, O.; Laiwattanapaisal, W. *Anal. Chim. Acta* **2013**, *788*, 39−45.

(4) Liu, H.; Crooks, R. M. *J. Am. Chem. Soc.* **2011**, *133*, 17564−17566.
(5) Renault, C.; Li, X.; Fosdick, S. E.; Crooks, R. M. *Anal. Chem.* **2013**, *85*, 7976−7979.
(6) Glavan, A. C.; Martinez, R. V.; Maxwell, E. J.; Subramaniam, A. B.; Nunes, R. M. D.; Soh, S.; Whitesides, G. M. *Lab Chip* **2013**, *13*, 2922−2930.
(7) Liu, H.; Li, X.; Crooks, R. M. *Anal. Chem.* **2013**, *85*, 4263−4267.
(8) Du, W.; Li, L.; Nichols, K. P.; Ismagilov, R. F. *Lab Chip* **2009**, *9*, 2286−2292.
(9) Maxwell, E. J.; Mazzeo, A. D.; Whitesides, G. M. *MRS Bull.* **2013**, *38*, 309−314.
(10) Martinez, A. W.; Phillips, S. T.; Whitesides, G. M.; Carrilho, E. *Anal. Chem.* **2009**, *82*, 3−10.
(11) Gubala, V.; Harris, L. F.; Ricco, A. J.; Tan, M. X.; Williams, D. E. *Anal. Chem.* **2011**, *84*, 487−515.
(12) Hu, J.; Wang, S.; Wang, L.; Li, F.; Pingguan-Murphy, B.; Lu, T. J.; Xu, F. *Biosens. Bioelectron.* **2014**, *54*, 585−597.
(13) Ge, L.; Wang, P.; Ge, S.; Li, N.; Yu, J.; Yan, M.; Huang, J. *Anal. Chem.* **2013**, *85*, 3961−3970.
(14) Lu, J.; Ge, S.; Ge, L.; Yan, M.; Yu, J. *Electrochim. Acta* **2012**, *80*, 334−341.
(15) Fu, E.; Kauffman, P.; Lutz, B.; Yager, P. *Sens. Actuators, B: Chem.* **2010**, *149*, 325−328.
(16) Ramachandran, S.; Fu, E.; Lutz, B.; Yager, P. *Analyst* **2014**, *139*, 1456−1462.
(17) Ge, S.; Ge, L.; Yan, M.; Song, X.; Yu, J.; Liu, S. *Biosens. Bioelectron.* **2013**, *43*, 425−431.
(18) Lewis, G. G.; Robbins, J. S.; Phillips, S. T. *Anal. Chem.* **2013**, *85*, 10432−10439.
(19) Wu, Y.; Xue, P.; Hui, K. M.; Kang, Y. *Biosens. Bioelectron.* **2014**, *52*, 180−187.
(20) Ruecha, N.; Rangkupan, R.; Rodthongkum, N.; Chailapakul, O. *Biosens. Bioelectron.* **2014**, *52*, 13−19.
(21) Dequaire, M.; Degrand, C.; Limoges, B. *Anal. Chem.* **2000**, *72*, 5521−5528.
(22) Liu, G.; Lin, Y.-Y.; Wang, J.; Wu, H.; Wai, C. M.; Lin, Y. *Anal. Chem.* **2007**, *79*, 7644−7653.
(23) Nie, Z.; Nijhuis, C. A.; Gong, J.; Chen, X.; Kumachev, A.; Martinez, A. W.; Narovlyansky, M.; Whitesides, G. M. *Lab Chip* **2010**, *10*, 477−483.
(24) Sönnichsen, C.; Reinhard, B. M.; Liphardt, J.; Alivisatos, A. P. *Nat. Biotechnol.* **2005**, *23*, 741−745.
(25) Carrilho, E.; Martinez, A. W.; Whitesides, G. M. *Anal. Chem.* **2009**, *81*, 7091−7095.
(26) Lu, Y.; Shi, W.; Jiang, L.; Qin, J.; Lin, B. *Electrophoresis* **2009**, *30*, 1497−1500.
(27) Pourbaix, M. *Atlas of electrochemical equilibria in aqueous solutions*; National Association of Corrosion Engineers, 1974.
(28) Bard, A. J.; Faulkner, L. R. *Electrochemical Methods: Fundamentals and Applications*; 2nd ed..; John Wiley & Sons: New York, 2001.
(29) Putnam, D. F. *Composition and Concentrative Properties of Human Urine*; National Aeronautics and Space Administration: Huntington Beach, CA, 1971.
(30) Yang, X.; Forouzan, O.; Brown, T. P.; Shevkoplyas, S. S. *Lab Chip* **2012**, *12*, 274−280.
(31) Szymanski, M. S.; Porter, R. A. *J. Immunol. Methods* **2013**, *387*, 262−269.
(32) De la Escosura-Muñiz, A.; Parolo, C.; Maran, F.; Mekoçi, A. *Nanoscale* **2011**, *3*, 3350−3356.
(33) Patel, M. N.; Wang, X.; Wilson, B.; Ferrer, D. A.; Dai, S.; Stevenson, K. J.; Johnson, K. P. *J. Mater. Chem.* **2006**, *20*, 390−398.
(34) Slanac, D. A.; Lie, A.; Paulson, J. A.; Stevenson, K. J.; Johnson, K. P. *J. Phys. Chem. C* **2012**, *116*, 11032−11039.